Progress in Nuclear Energy 190 (2026) 105986

Contents lists available at ScienceDirect

Progress in Nuclear Energy

journal homepage: www.elsevier.com/locate/pnucene

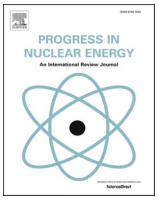

Improving sinterability of UO_2-Gd_2O_3 fuel pellets by high-energy mixing

Artur Cesar Freitas [a], Diogo Ribeiro Costa [b], Ricardo Mendes Leal Neto [a], Elita Fontenele Urano de Carvalho [a], Michelangelo Durazzo [a,*]

[a] Nuclear and Energy Research Institute – IPEN/CNEN-SP, São Paulo, Brazil
[b] Westinghouse Electric Sweden AB, Västerås, Sweden

ARTICLE INFO

Keywords:
Nuclear fuel
Uranium
Gadolinium
Burnable poison
Homogeneity

ABSTRACT

The optimization of nuclear fuels for use in pressurized water reactors can be achieved by increasing the burnup cycle. One way to achieve these goals is to anticipate an initial excess of reactivity in the reactor design and incorporate so-called burnable poisons directly into the fuel to control the neutron population. Due to its neutronic properties, gadolinium is one of the main elements incorporated in the form of oxide (Gd_2O_3). The dry mechanical mixing of UO_2 powder and Gd_2O_3 is the commercially most attractive method due to its simplicity. However, this method leads to challenges in obtaining sintered pellets with high sintered density for use in nuclear reactors due to the Kirkendall effect. In this work, 10 wt% of Gd_2O_3 powder was added to UO_2 powder through dry mechanical mixing in low- (Turbula®) and high-energy (SPEX®) mixers. The powders were homogenized in turbula mixer for 1 h and 80 h. The mixing time did not improve the sintered density, which were about 91.5 % of theoretical density (TD). Homogenizations in the SPEX mixer were carried out at 15, 30, and 60 min. The highest sintered densities in this case were 95.8 % and 96.3 % TD achieved with 30 min and 60 min, respectively. Mixing the powders through a process involving more intense agitation allows for the breaking of Gd_2O_3 clusters without significant changes in the properties of UO_2, thus improving the sinterability of the UO_2-Gd_2O_3 fuel pellet.

1. Introduction

The UO_2-based nuclear fuel derived from the AUC (ammonium uranyl carbonate) route is widely used in Light Water Reactors (LWRs) (Campolina et al., 2018). The advantage of this route is the production of UO_2 powder with good flowability, as well as having particle size and specific surface area suitable for direct pressing without the need of intermediate granulation steps (Santos et al., 2017).

Increasing the fuel lifetime has been a recognized need since commercial nuclear energy generation began. Extending fuel burnup, reducing reload intervals, and decreasing costs associated with final storage of radioactive waste are crucial elements in minimizing the costs involved in the fuel cycle. Fuel optimization involves increasing initial reactivity. To mitigate the high initial reactivity, neutron-absorbing materials have been employed to control neutron population.

Neutron-absorbing materials, also known as burnable poisons, have high neutron absorption cross-sections, while transmutation products (isotopes) should have negligible cross-sections. These low values mean that the reaction product between the absorber material and neutron has low neutron absorption capacity. Thus, the neutron absorption capacity of the burnable poison depletes as the reactor's initial reactivity decreases.

One way of using a burnable poison is by directly integrating it into nuclear fuel. The most used chemical element for this purpose is gadolinium in oxide form (Gd_2O_3). Its use as a burnable poison began in the 1960s, and its successful performance in this type of fuel has led to its widespread use by most suppliers, with concentrations ranging from 6 to 10 wt% (IAEA,1995). The Brazilian reactor Angra-2 utilizes pellets with up to 7 wt% of Gd_2O_3 mixed with UO_2 (Campolina et al., 2018).

The nuclear fuel components UO_2 and Gd_2O_3 are particulate materials with high melting temperatures. Uniformity in powder mixing ensures that the final pellet has consistent properties. The better dispersed the gadolinium is in the UO_2 matrix, the more predictable its behavior will be in subsequent manufacturing steps, leading to better uniformity in neutron properties during irradiation.

The incorporation of gadolinium into UO_2 can be achieved by

* Corresponding author. Av. Prof. Lineu Prestes, 2242, Cidade Universitária, CEP 05508-000, São Paulo, SP, Brazil.
E-mail addresses: arturcfr@gmail.com (A.C. Freitas), diogo.ribeirocosta@westinghouse.com (D.R. Costa), lealneto@ipen.br (R.M. Leal Neto), elitaucf@gmail.com (E.F. Urano de Carvalho), mdurazzo@ipen.br, mdurazzo@usp.br (M. Durazzo).

https://doi.org/10.1016/j.pnucene.2025.105986
Received 25 April 2025; Received in revised form 5 August 2025; Accepted 13 August 2025
Available online 15 August 2025

various processes aiming homogeneous distribution. The way Gd_2O_3 is dispersed in the UO_2 matrix impacts the sintering behavior, resulting in different density levels. Homogeneity can be divided into three levels (Durazzo and Riella, 2001). First, the highest degree of homogeneity is achieved with the atomic level distribution of gadolinium, where the chemical elements composing the nuclear fuel form a solid solution in the resulting powder particles. This process occurs when the mixed powder is prepared using the coprecipitation technique via ADU (ammonium diuranate). Second, the intermediate level, also known as the microscopic level of homogeneity, occurs when UO_2 and Gd_2O_3 precipitate simultaneously without forming a solid solution. However, each powder particle contains both chemical elements. This powder is obtained through the coprecipitation technique via AUC, which ensures homogeneity at the molecular level. Third, at the macroscopic level of homogeneity, the powders are mixed mechanically in a dry state. The powder dispersion occurs heterogeneously, forming clusters of materials that are close to each other but without chemical affinity.

Despite the low level of homogeneity, the process of dry mechanical mixing of Gd_2O_3 with UO_2 powder from AUC is the most commercially attractive process due to its simplicity and the absence of intermediate steps for pelletizing and sintering (Manzel and Dörr, 1980). Furthermore, the addition of Gd_2O_3 through this process does not cause a significant alteration in the production line of nuclear fuel via AUC.

The manufacturing process of these pellets on an industrial scale requires automatic feeding of the compaction presses. The powder is filled into the dies for compression by the punches. The obtained powder needs to have good “incipient flow” (transition from static to dynamic state) and “dynamic flow” properties to obtain reproducible and homogeneous pellets in the industrial environment (Beaunac et al., 2022). The high flowability of UO_2 powder via AUC allows for dry mechanical homogenization of quantities up to approximately 2000 kg with up to 20 % by weight of Gd_2O_3 (Assmann et al., 1988).

The turbula is a commonly used mixer in research and development. This mixer facilitates smooth and continuous movements, enabling mixture homogeneity. Some studies indicate mixing times of 3 h (Mills et al., 1989) or 4 h (Pagano et al., 2008), while others report 1 h of mixing (Restivo et al., 2004; Durazzo et al., 2018). There is no standardization in the reported times and justification in the articles for the mixing times in turbula.

After the powder mixture, the material is compacted into a pellet shape and sintered. In this process, the Gd_2O_3 and UO_2 powders form a substitutional solid solution, where U^{4+} cations are substituted by Gd^{3+} in reducing atmospheres (Ho and Radford, 1985; Song et al., 2001; Durazzo et al., 2010; Balakrishna, 2016). When the trivalent cation Gd^{3+} is incorporated into the UO_2 lattice in place of the U^{4+} cation, the resulting effective charge from the site where the substitution occurred is -1. To maintain the electronic neutrality of the host lattice, a $+1$-charge variation is required, which can be achieved by the transition of uranium valence, occupation of the same cation in interstitial positions, or alteration in the internal lattice formed by oxygen, which can gain or lose the anion O^{2-}. The characteristics of Gd^{3+} ions in terms of their ionic radius, valence, and the crystal structure of Gd_2O_3 contribute to facilitating the formation of a solid solution with UO_2, as established by the Hume-Rothery rules (Hume-Rothery, 1966). The ionic radius of U^{4+} is 0.1011 nm, while Gd^{3+} is 0.1053 nm (Fedotov et al., 2013), resulting in a difference of 4.15 % between the mentioned ionic radii.

The sintering atmosphere is primarily responsible for the principal charge compensation mechanism. In H_2 reducing atmospheres, there is a good agreement among various authors in studies published since the 1980s that the incorporation of the Gd^{3+} cation into the UO_2 crystal lattice causes a linear decrease in the lattice parameter (Fukushima et al., 1982; Hirai and Ishimoto, 1991; Leyva et al., 2002; Cardinaels et al., 2012; Baena et al., 2015). The shrinkage in the lattice parameter is mainly due to the charge compensation mechanism and occurs up to the addition of 50 mol% of Gd_2O_3 (Durazzo and Riella, 2009). U cations for U^{5+} and U^{6+} valences have smaller atomic radii (0.084 nm and 0.081 nm, respectively (Shannon, 1976), justifying the decrease in the lattice parameter of the structure.

If the dry mechanical mixing of both the UO_2 and Gd_2O_3 powders is not efficient, the inhomogeneity of mixed powders leads to problems ranging from decreased density to the microstructure of the matrix. Pellets manufactured from mixed powders cause variation in the local concentration of chemical elements. Riella et al. (1991) conducted the sintering of a UO_2-7.5 wt%Gd_2O_3 mixture made with pellets prepared with an atomic level of homogeneity through the coprecipitation method and another pellet prepared with a macroscopic level of homogeneity through mechanical mixing. While the first sample showed a uniform distribution of the burnable poison, the sample made by mechanical mixing showed regions with up to 25 wt% of Gd_2O_3.

Leyva et al. (2002) analyzed the influence of mixing by X-ray diffraction (XRD) of heterogeneous mixtures. Through Rietveld method analysis, two phases of the same fluorite lattice with different lattice parameters were detected in the same sample, showing a concentration difference along the UO_2 matrix. In the sample prepared by dry mixing with 8 wt% Gd_2O_3, lattice parameters of 0.54704 nm and 0.54308 nm were detected. The first value is consistent with the decrease in the lattice parameter when gadolinium is added in this proportion, but the second one does not follow the Vegard’s law, suggesting the formation of a new phase in microregions.

Based on diffusion pair experiments conducted at the interfaces of UO_2 and Gd_2O_3, as reported by Durazzo et al. (2010), an asymmetrical interdiffusion behavior was observed. Specifically, gadolinium exhibited significant diffusion into the UO_2 matrix, whereas uranium demonstrated minimal penetration into the Gd_2O_3 crystal structure. This disparity in diffusion rates suggests a misbalance between the species, potentially attributable to differences in their respective diffusion coefficients and solubility limits within the host lattices. This asymmetric interdiffusion phenomenon, known as the Kirkendall effect, arises due to the higher diffusivity of Gd^{3+} cations into the UO_2 matrix relative to the significantly slower diffusion of U^{4+} ions into Gd_2O_3. As a result, the initial sites occupied by Gd_2O_3 aggregates become depleted, leading to the formation of voids. These voids, generated at elevated temperatures during the sintering process, are challenging to eliminate and contribute to the development of so-called Kirkendall pores. Thus, there is a concentration of the burnable poison around Kirkendall pores (Durazzo et al., 2013; Balakrishna, 2016), probably modifying the lattice parameter in microregions of the pellet.

In the sintering of pellets with mixed powders, a solid solution is formed simultaneously with the densification process. Gd_2O_3 solubilizes in the UO_2 structure faster than the opposite, leaving voids where clusters of gadolinia particles were initially located. Gd_2O_3 tends to form clusters that are difficult to break. The formation of a solid solution in mixtures of low homogeneity levels generates pores due to the Kirkendall effect, thus reducing the density of the sintered pellets.

Durazzo et al. (2013) manufactured UO_2- Gd_2O_3 pellets using Gd_2O_3 agglomerates selected by size range. The pellets were prepared with agglomerates classified into sizes <37 μm, 37–45 μm, 45–53 μm, and 53–62 μm. The mixtures were prepared in a Turbula mixer, pressed and sintered for 3 h in a hydrogen atmosphere. The analysis of the four pellets showed a progressively increasing average pore size, demonstrating the occurrence of the Kirkendall effect. In the pellets with agglomerates above 45 μm, free Gd_2O_3 was identified, indicating incomplete dissolution. These findings highlight the critical influence of Gd_2O_3 distribution homogeneity within UO_2-Gd_2O_3 fuel pellets on sintering behavior. Specifically, reduced homogeneity in gadolinium oxide dispersion correlates with lower final sintered densities, likely due to the formation of Kirkendall pores at sites previously occupied by Gd_2O_3 agglomerates. These pores, resulting from differential diffusion rates between gadolinium and uranium during sintering, impede densification and persist in the final pellet structure.

These results suggest that a more comprehensive investigation into the influence of mechanical mixing parameters—specifically mixing

Table 1
Nomenclature, route, and mixing time for mixtures of UO_2-Gd_2O_3 powders.

Pellets	Route	Time
T1	LEM	1 h
T80	LEM	80 h
S15	HEM	15 min
S30	HEM	30 min
S60	HEM	60 min

time and energy—on the sintering behavior and microstructural evolution of UO_2–Gd_2O_3 pellets is warranted. In this study, dry mixing routes for UO_2 and Gd_2O_3 powders are compared using both low- and high-energy mixing devices. The results showed that the mixture obtained via high-energy mixing preserves the favorable morphological features of the UO_2 powder derived from the AUC process (notably, high flowability) and mitigates the Kirkendall effect. This facilitates adequate densification and yields a satisfactory microstructure when subjected to conventional sintering.

2. Experimental

2.1. Raw materials

The Nuclear Industries of Brazil (INB) provided the UO_2 powder used in this study, which was manufactured by an industrial AUC route (Costa et al., 2013). The Gd_2O_3 powder was provided by the Navy Technological Center - (CTM) Aramar/SP. For assistance in compacting the UO_2 and UO_2-Gd_2O_3 pellets, aluminum distearate (ADS, supplied by INB) and zinc stearate (Quimesp brand) were used as solid lubricants.

The UO_2 powder was characterized for specific surface area (BET), apparent density, moisture content, O/U ratio, and trace impurities. Gd_2O_3 underwent the same analyses, except for the O/U ratio. The morphological characteristics of UO_2, Gd_2O_3, and ADS powders were examined using a Thermo Fisher Prisma E scanning electron microscope (SEM) with secondary electron detector (SE). Particle size distributions were measured by laser diffraction using CILAS laser equipment (model 1064), with water as the liquid medium and tetrasodium pyrophosphate as the dispersing agent. The width of the distribution is measured by the span index. The narrower the distribution, the lower the span value, which is calculated by equation (1).

$$span = \frac{D90 - D10}{D50} \quad (1)$$

where D10, D50 and D90 are the volume-based percentile diameters which represent 10, 50 and 90 % of the particle size, respectively.

2.2. Preparation of powder mixtures with low- and high-energy mixers

UO_2-10 wt%Gd_2O_3 powders we mixed using two types of equipment: a low-energy mixer and a high-energy mixer. The low-energy mixer (LEM) utilized was from Wab Turbula brand, model T2F, with a rotation of 48 rpm. Interlaced wires were used inside the homogenization vessel to promote the breaking of agglomerates. The powders were mixed in batches of 50 g, with mixing times of 1 h and 80 h. The high-energy mixer (HEM) was from Spex Sample Prep., model 8000M Mixer/Mill, with a rotation of 1425 rpm. The powders were placed in an AISI 304 steel container in batches of 50 g. Samples were mixed for 15, 30, and 60 min. In both experimental setups, no mixing aids—such as grinding balls or other mechanical artifacts—were introduced during the blending process.

Before the mixing, Gd_2O_3 powder was heated to 100 °C for 1 h to remove moisture. In all samples, ADS concentration was 0.2 wt%, following the standard procedure adopted by INB (Costa and Freitas, 2017; Jentzen and Didway, 1990). Powders were weighed on an analytical balance, Shimadzu brand, with a precision of 0.0001 g.

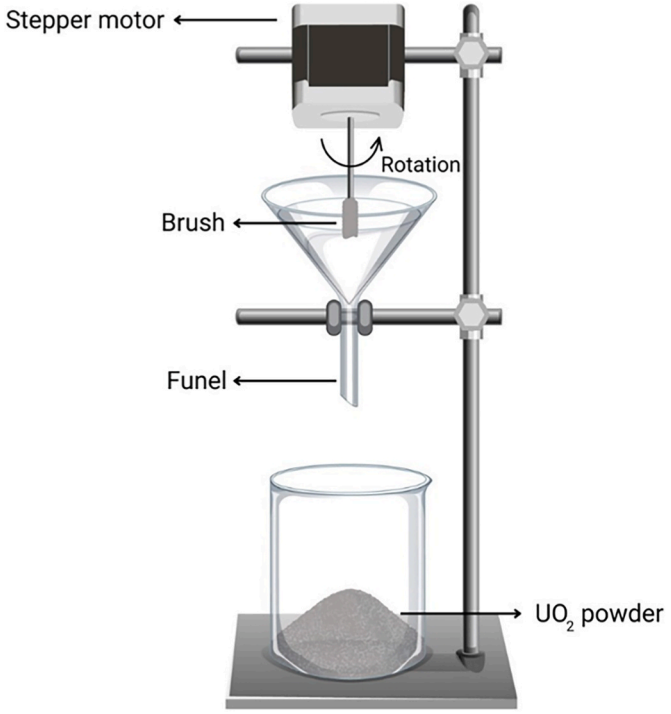

Fig. 1. Schematic representation of the powder flowability measurement apparatus.

Several samples were homogenized by the dry mechanical method using LEM (T series) and HEM (S series) routes. Table 1 shows the sample nomenclatures, routes, and associated times.

The flowability of the mixtures is an essential parameter for their industrial use, as the automatic feeding of compaction matrices depends on this parameter. To evaluate the influence of high-energy mixing on the flowability of UO_2 powder, samples of pure UO_2 were subjected to mixing durations of 15, 30, and 60 min. Subsequent to each mixing interval, the flowability was assessed by introducing 50 g of the processed powder into a glass funnel with a 7 mm orifice diameter. A rotating brush was placed near the funnel cavity, operated by a stepper motor programmed at 100 rpm. After positioning the powder, the flow time was quantified. This procedure was repeated five times to collect statistical data. Fig. 1 shows a schematic representation of the device used to measure the flowability of the UO_2 powder. This method is similar to that adopted by INB. Since flowability depends on the powder morphology, the morphology was also evaluated by SEM after homogenization.

To calculate the confidence interval of flowability (E), the Student's T-table was used with 4 degrees of freedom and a confidence level of 0.95, according to the following equation (2):

$$E = \overline{X} \pm t\frac{\sigma}{\sqrt{n}} \quad (2)$$

where, $\overline{X}$ is mean flow times, t is value given by the Student's T-table (t = 2.132), σ is standard deviation of flow times and n is number of repetitions (n = 5).

For determination of apparent density, the same device was used, but the powder was collected in a container with a defined volume of 25 mL. The powder flows until the container is completely filled. Excess powder is removed with a spatula. Apparent density is determined by the ratio of mass to the volume of 25 mL.

2.3. Pressing, sintering, and pellet characterization

The samples were pressed in a cylindrical die with an internal

Table 2
Some physicochemical data for UO_2.

Characteristics	Results	Specification[a]
O/U	2.08	2.08–2.30
U_{total} (%)	87.6	≥86.8
Enrichment U-235 (%)	4.137	4.10–4.15
Moisture (wt%)	0.15	≤0.4
Surface area (m^2/g)	5.0	2.5–6.0
Bulk density (g/cm^3)	2.2	2.0–2.6
Flowability (s/50g)	4.6	≤10
D50 (μm)	23.6	<200
Impurities (μg/g)		
F	5.312	≤100
Al	1.777	≤250
Ca	4.212	≤25
B	<0.2	≤0.5
Fe	15.24	≤100
Ni	0.421	≤50
Si	6.916	≤100
Gd	0.2	≤1

[a] Specification for the UO_2 powder manufactured by INB for the Brazilian PWR type ANGRA-1 and ANGRA-2 reactors.

diameter of 10 mm, using a pressure of 350 MPa. The densities of the green pellets, i.e. green densities, were determined geometrically. The height and diameter were determined using a caliper with a precision of 0.01 mm. The theoretical density (TD) of the mixture was calculated considering theoretical densities of 10.96 g/cm^3 for UO_2 (Fedotov et al., 2013), 7.41 g/cm^3 for Gd_2O_3 (Balakrishna, 2016), and 1.01 g/cm^3 for ADS (Yaws, 2015). The pressing pressure was adjusted to obtain a green density of 50 %TD (Coleman and Beeré, 1975).

Sintering of the samples was conducted using a Setaram Setsys 1700 dilatometer at 1700 °C for 240 min under a pure hydrogen atmosphere. The heating rate was maintained at 5 °C/min. Sintered densities were determined via the Archimedes principle (immersion method), by weighing the samples while immersed in water.

According to IAEA specifications (International Atomic Energy Agency IAEA, 1995), the density of sintered UO_2–Gd_2O_3 fuel pellets must be within the range of $95\ ^{+1.0}_{-1.5}$ % of the theoretical density (TD), corresponding to a total porosity (sum of open and closed pores) between 4.0 % and 6.5 % by volume.

The total porosity was evaluated using the following equation based on the immersion method:

$$\rho = \frac{m_{dry}}{m_{dry} - m_{wet}} . \rho_{water} \tag{3}$$

where: m_{dry} is the mass of the dry pellet in air (g), m_{wet} is the apparent mass of the pellet when submerged in water (g), and ρ_{water} is the density of water at the measurement temperature (g/cm^3).

The analytical balance used had a precision of 0.5 mg, and the maximum measurement uncertainty in determining the pellet density was estimated to be 0.02 g/cm^3.

The theoretical density D_{th} of the UO_2–Gd_2O_3 composite was calculated using the rule of mixtures, as follows:

$$D_{th} = \frac{100}{\frac{\%Gd_2O_3}{D_{th}Gd_2O_3} + \frac{\%UO_2}{D_{th}UO_2}} \tag{4}$$

where: $\%Gd_2O_3$ and $\%UO_2$ are the weight percentages of Gd_2O_3 and UO_2 in the mixture, respectively, $D_{th}Gd_2O_3 = 8.33$ g/cm^3 is the theoretical density of monoclinic Gd_2O_3 (American Society for Testing and Materials, 2021), and $D_{th}UO_2 = 10.96$ g/cm^3 is the theoretical density of UO_2 (American Society for Testing and Materials, 2021).

After sintering, microstructural characterization was performed by SEM on polished sections of the pellets. Samples were sequentially ground with 400 and 1200 grit sandpaper and polished with 3 μm and 1 μm diamond suspension. Afterwards, SEM analyses were performed by a Thermofisher SEM (Prisma E), using secondary electrons for image formation and an EDS detector for chemical composition verification. Due to this technology, it was possible to identify the position of atoms at specific points, in line, and in a field, allowing the production of uranium and gadolinium chemical maps with a count of 120 min at 15 kV.

Table 3
Some physicochemical data for Gd_2O_3 powder.

Characteristics	Results
Gd content (%)	84.2
D50 (nm)	4.2
Surface area (m^2/g)	1.5
Bulk density (g/cm^3)	2.4
Moisture (wt%)	0.32
Impurities (μg/g)	
CaO	0.8
Fe_2O_3	0.4
SiO_2	0.6
Dy_2O_3	<1
Eu_2O_3	5.1
Sm_2O_3	2.7
Y_2O_3	<1

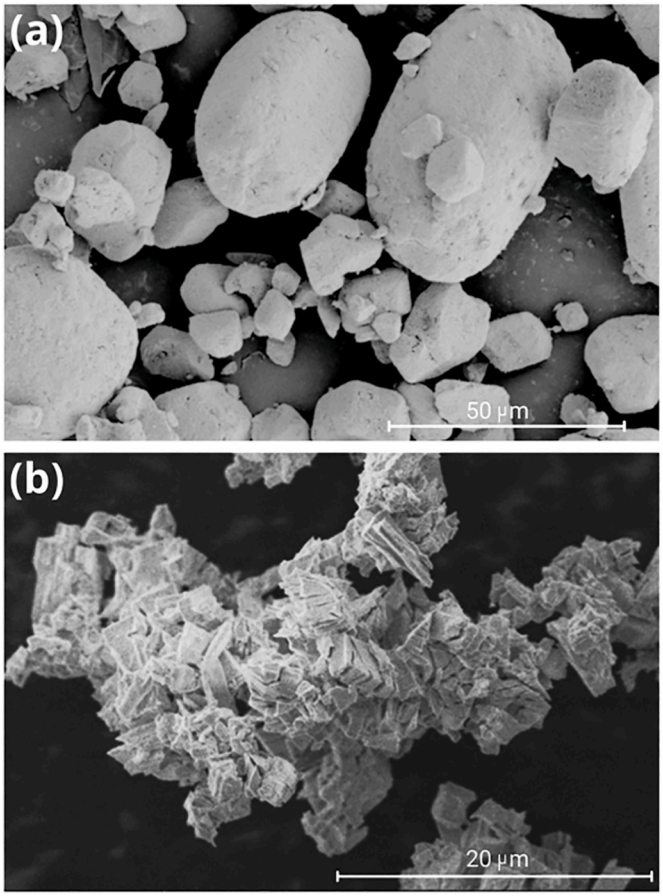

Fig. 2. SEM micrograph with secondary electron detector. a) UO_2 powder. b) Gd_2O_3 powder.

3. Results and discussion

3.1. Physical and chemical characterization of raw materials

The raw materials used in this work were chemically and physically characterized. Tables 2 and 3 present the results obtained for UO_2 and Gd_2O_3 powders, along with the specification values from the standard

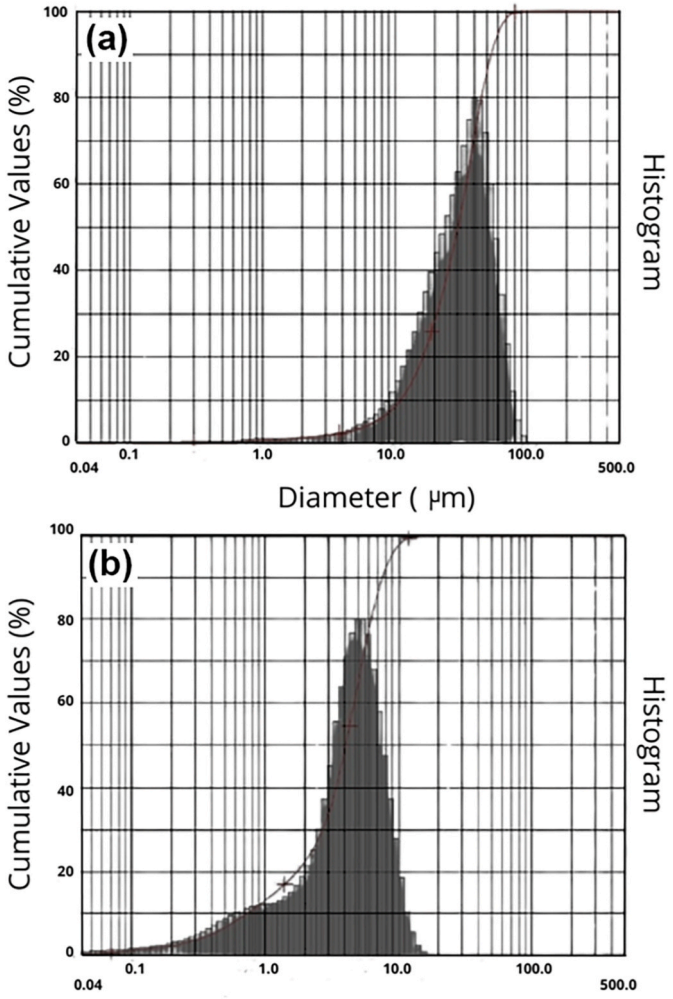

Fig. 3. Particle size distribution of UO_2 (a) and Gd_2O_3 (b) powders.

used at INB as a reference Costa et al. (2013).

The supplied Gd_2O_3 has a purity of 99.88 %, and no traces of impurities greater than specified were identified in the UO_2 powder. The presence of impurities in UO_2 and Gd_2O_3 can lead to phase formation during sintering and accumulation at grain boundaries, forming gaps that can result in intergranular cracking (Radford and Pope, 1983). Additionally, impurities with high absorption cross-sections can modify the neutronic performance of the nuclear fuel.

Fig. 2a illustrates the morphology of the UO_2 powder. Various particle sizes can be observed (~2–100 μm), with some particles being faceted (smaller particles) and others having rounded corners. This morphological characteristic provides good flowability to the powder and is typical of manufacturing via AUC (Choi et al., 1988). Fig. 2b shows the morphology of the Gd_2O_3 powder. Irregular, angular particles with sharp corners and crystals with smooth surfaces can be observed in the image. Gd_2O_3 has a high tendency to agglomerate, forming cohesive structures.

Fig. 3 displays the particle size distribution of the UO_2 (Fig. 3a) and Gd_2O_3 (Fig. 3b) powders. UO_2 exhibits a monomodal distribution, with a D50 value of 23.6 μm. The Gd_2O_3 powder size distribution reflects a combination of particles that detached and others that remained in agglomerates. Gd_2O_3 shows a bimodal distribution with two peaks, indicating populations with values close to 1 and 10 μm. The determined D50 value is 4.2 μm.

Table 4
Particle sizes and span indexes of original UO_2 powder and samples subjected to the high-energy mixer for 15, 30, and 60 min.

Shacking time	D10 (μm)	D50 (μm)	D90 (μm)	Span
0 min (original UO_2)	10.0	23.6	54.0	1.9
15 min	9.8	22.5	50.9	1.8
30 min	9.8	21.1	46.5	1.7
60 min	9.7	21.1	45.6	1.7

3.2. *Influence of high-energy mixing on UO_2 powder morphology and flowability*

The high-energy mixing process increases the frequency and intensity of collisions among particles and between particles and the mixing vessel walls. These energetic interactions are anticipated to effectively disintegrate Gd_2O_3 agglomerates, resulting in a more homogeneous mixture compared to low-energy mixing methods. However, it is crucial that this process does not cause significant fragmentation of UO_2 particles, thereby preserving the original powder's flowability. To assess the impact of high-energy mixing on particle size distribution, morphology, and flowability, pure UO_2 powders were subjected to this mixing technique and subsequently characterized.

Table 4 shows the particle size data of the original UO_2 powder particles and those shacked in the HEM for 15, 30, and 60 min. The span indexes indicate narrowing in the particle size distributions, with larger particles experiencing more significant changes. The D90 value of sample S60 decreased by 13.9 % compared to the original powder and no significative changes was observed on D10 values.

Scanning Electron Microscopy (SEM) analysis revealed no discernible alterations in the morphology of the original UO_2 powder following exposure to high-energy mixing, as depicted in Fig. 4.

Variations in powder flowability were observed following high-energy mixing (HEM), as depicted in Fig. 5. The observed decrease in flow time for 50 g of powder with increasing mixing duration indicates an enhancement in powder fluidity. Powder flowability occurs due to gravitational forces and cohesive forces between particles (van der Waals force). In fine particles, cohesive forces are more relevant and, therefore, an increase in their quantity decreases the flowability of UO_2 powder (Madian et al., 2020). The agitation process caused a decrease in particle size but without changing D10 (fine particles) significantly. Larger particles typically exhibit superior flowability due to the dominance of gravitational forces over cohesive interparticle forces. In this study, although a reduction in the D90 value was observed with increased mixing time, this decrease was insufficient to adversely affect the powder's flowability. This outcome suggests that the extent of particle size reduction did not significantly enhance cohesive interactions to a level that would impede flow. The improvement in flowability indicates that particle rounding likely occurred, facilitating fluidity.

Table 5 presents the bulk density data of the same powders used in the flowability measurement. The results indicate an increase in density as the mixing time increases. This is due to the decrease in D90 and smoother granules, resulting in better packing of powders that spent more time in the mixer.

The variation in the powder particle size is important for studying the characteristics that determine flowability, compactability, and sinterability. There are advantages and disadvantages regarding the presence of fine particles. On one hand, powders with a large fraction of small particles, besides having lower flowability, are more difficult to compact. On the other hand, fine particles have higher specific surface and are easier to sintering, resulting in pellets with higher density after sintering (Glodeanu et al., 1988). Additionally, the presence of fines has a lubricating effect during pressing (Fruhstorfer and Aneziris, 2017). Thus, a balance in particle distribution is essential to ensure that the powder exhibits good flowability and green density, which result in sintered densities high enough to be within the specification limits for

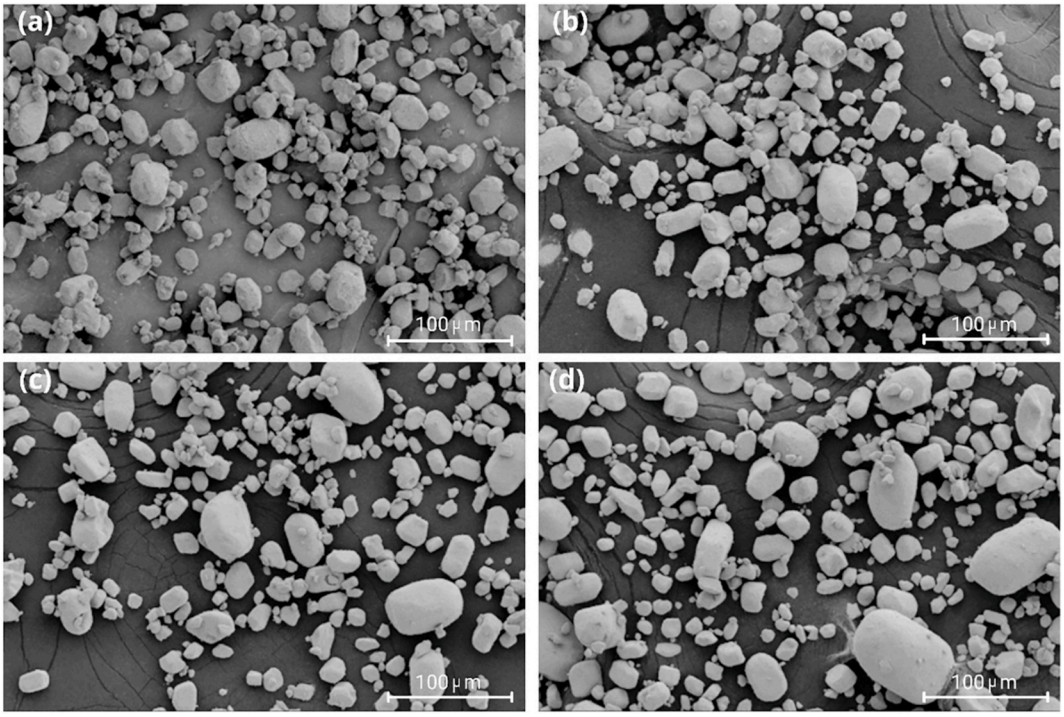

Fig. 4. SEM images of the original UO_2 powder (a) and after shacking in the HEM for 15 min (b), 30 min (c), and 60 min (d).

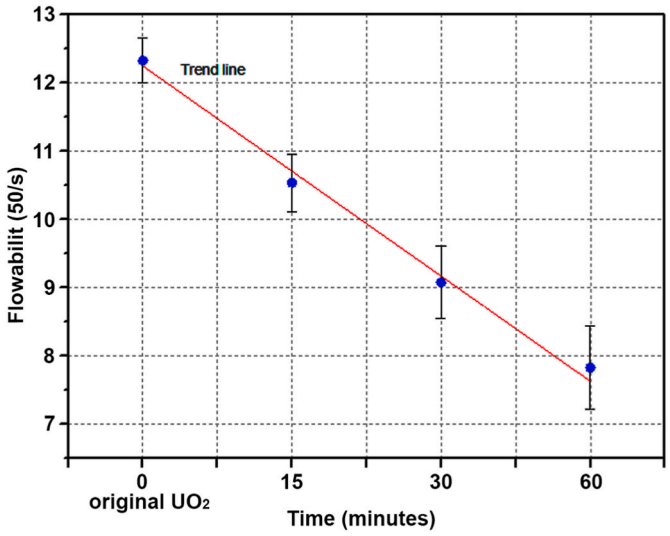

Fig. 5. Flowability of original UO_2 powder and after shacking in HEM for 15, 30, and 60 min.

Table 5
Bulk density of original and UO_2 powders after shacking in the HEM for 15, 30, and 60 min.

Shacking time (min)	Bulk density (g/cm^3)
0 (originalUO_2)	2.36 ± 0.02
15	2.40 ± 0.03
30	2.47 ± 0.03
60	2.54 ± 0.03

Table 6
Geometric density of green pellets.

Pellet	Green density (g/cm^3)	TD of the mixture (g/cm^3)	% TD
original UO_2	5.41 ± 0.05	10.75	50.3 ± 0.4
T1	5.12 ± 0.04	10.27	49.9 ± 0.4
T80	5.15 ± 0.02	10.27	50.2 ± 0.2
S15	5.13 ± 0.03	10.27	50.0 ± 0.3
S30	5.11 ± 0.05	10.27	49.8 ± 0.5
S60	5.15 ± 0.04	10.27	50.2 ± 0.4

nuclear fuel application.

3.3. Pressing and sintering

After mixing in the LEM and HEM, the homogenized powders containing 0.2 wt% ADS (solid lubricant) were pressed to obtain green pellets with 50 ± 0.5 % TD (theoretical density) of the mixture. Table 6 presents the green densities of all mixtures.

Fig. 6a shows the sintering behaviors of T1 and T80 of UO_2-Gd_2O_3 samples. The pure UO_2 pellet retracted continuously until reaching a temperature near 1700 °C. The addition of Gd_2O_3 reduces the total pellet shrinkage by dry mixing in LEM (low-energy mixing). Sintering blockage occurs due to the Kirkendall effect, in which Gd_2O_3 clusters dissolve in the UO_2 matrix and leave pores behind. Thus, this pore formation delays pellet shrinkage and causes an inflection in the sintering curve, as seen in Fig. 6a. The typical sintering blockage of the mixtures are observed at temperatures close to 1200 °C, as already observed in previous works (Durazzo et al., 2010, 2013; Yuda and Une, 1991; Kim et al., 2001).

Fig. 6b reports the pellet shrinkage rate of UO_2 pellets, T1 and T80 (low-energy mixing). With the addition of Gd_2O_3, two peaks occur. The first peak coincides with the beginning of solid solution formation. At this temperature range, there is an expansion of the UO_2 matrix to accommodate gadolinium atoms while forming voids in the place of the Gd_2O_3 clusters, resulting in two simultaneous effects. When solid solution formation is completed, the retraction rate increases again.

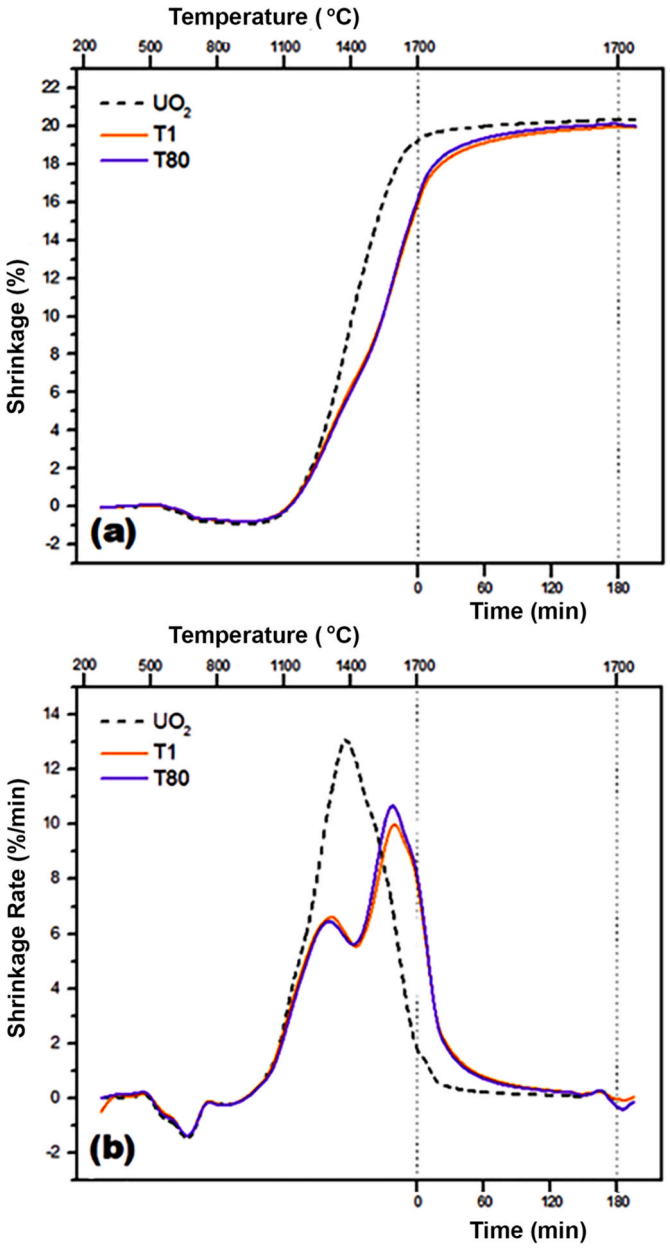

Fig. 6. Shrinkage curves of UO_2 and UO_2-10 wt% Gd_2O_3 pellets, mixed in the LEM for 1 h (T1) and 80 h (T80): (a) linear shrinkage, (b) shrinkage rate.

However, the completion of solid solution formation creates stable pores, which are formed by the Kirkendall effect at high temperatures and are hardly closed until the end of the sintering process.

The results in Fig. 6 indicate that the mixing time in LEM did not affect the sintering behavior significantly. This likely occurred due to the mechanical resistance of the clusters, which did not break during mixing in turbula, even for long homogenization times (80 h).

Fig. 7 highlights a Kirkendall pore originated from a Gd_2O_3 cluster in sample T1. The gadolinium concentration (Fig. 7b) presented in the EDS line analysis (Fig. 7a) is higher at the pore edges, when compared to the bulk, while the uranium concentration is higher in the bulk and lower at the pore edges. The EDS map of Gd (Fig. 7c) also shows higher concentration of Gd around the pores, which were originally Gd_2O_3 particles/clusters and, during sintering, were dissolved in the UO_2 matrix over short distances.

Fig. 8 presents the elemental mapping of gadolinium distribution in sintered UO_2-Gd_2O_3 pellets prepared via the low-energy mixing (LEM)

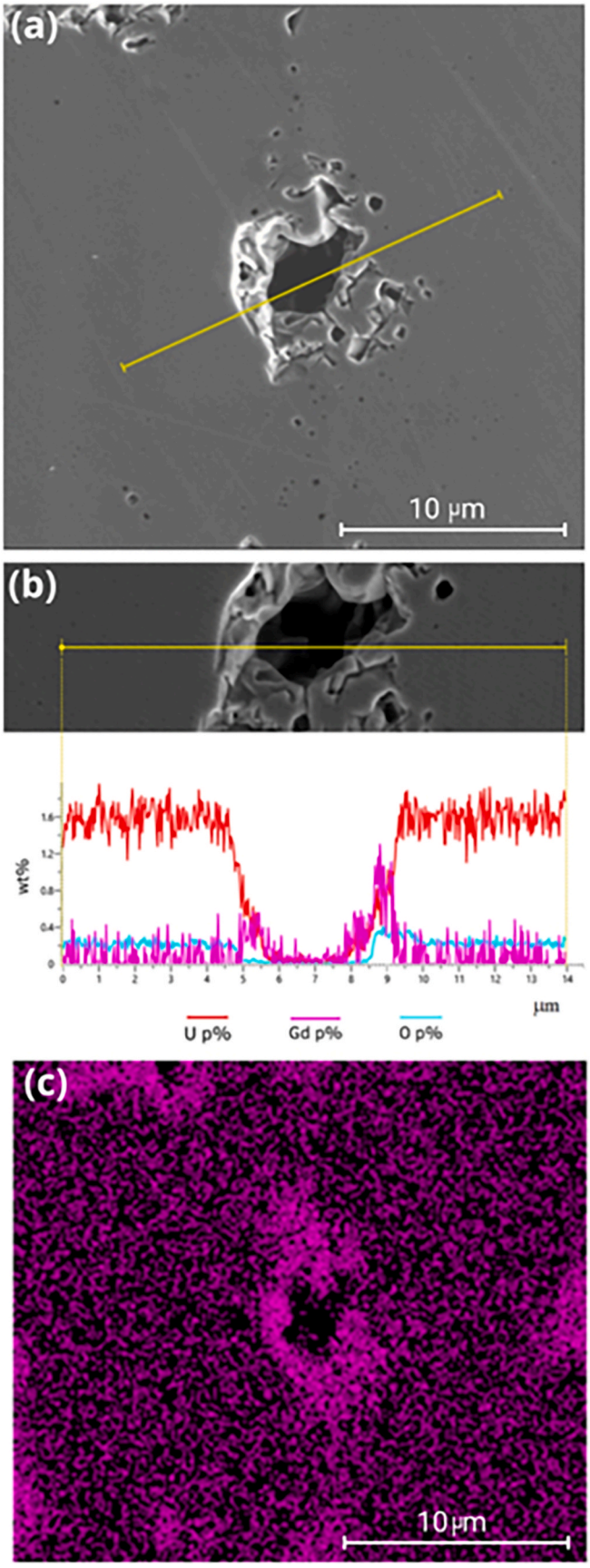

Fig. 7. Analysis of a pore in the $(U,Gd)O_2$ pellet (T1 sample): (a) SEM image of the pore with a line drawn for EDS analysis; (b) uranium and gadolinium concentration; (c) EDS mapping.

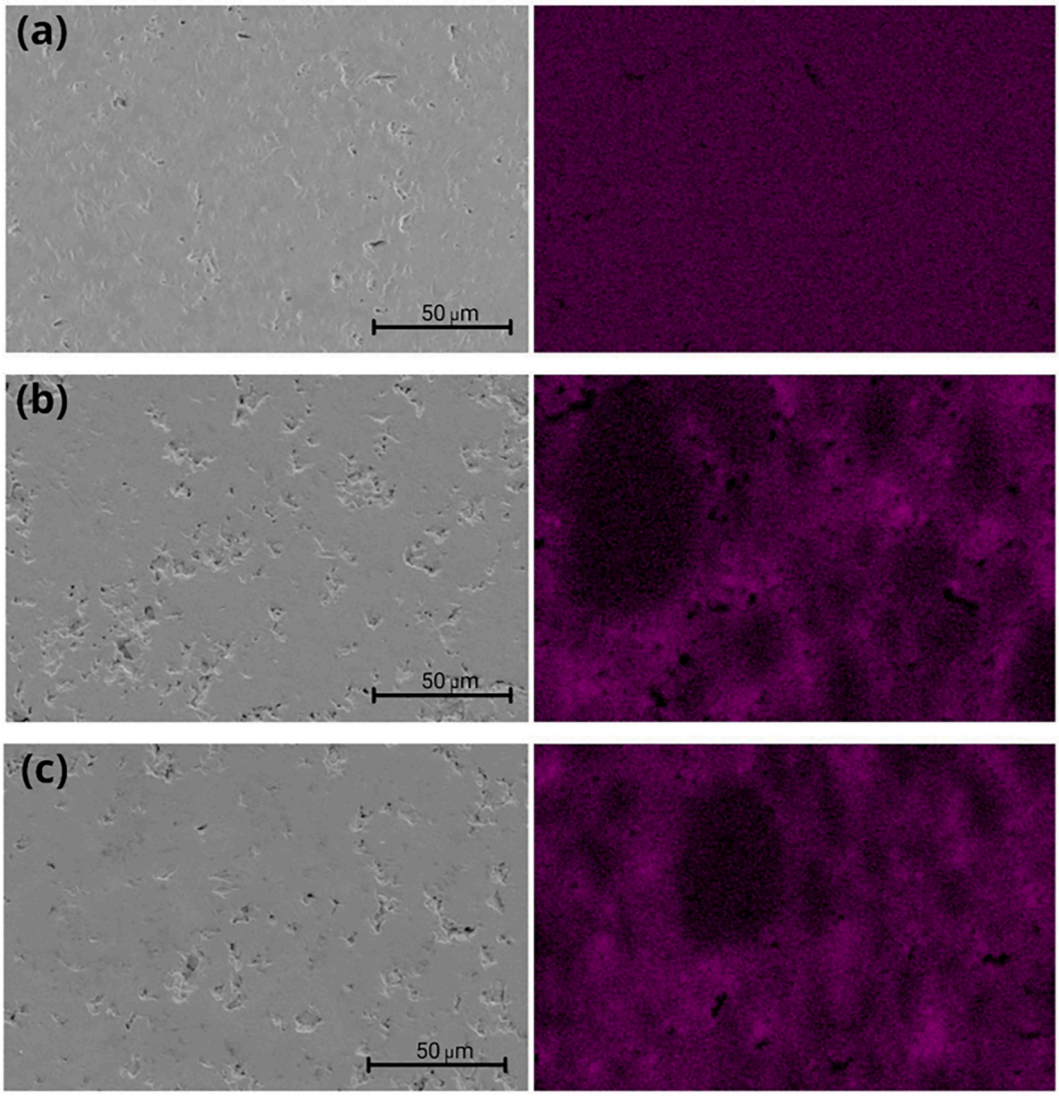

Fig. 8. SEM micrograph with secondary electron detector and EDS mapping of the pure UO_2 pellet (a), UO_2-Gd_2O_3 pellet T1 (b), and UO_2-Gd_2O_3 pellet T80 (c).

route. Energy-dispersive X-ray spectroscopy (EDS) analyses reveal significant heterogeneity in gadolinium dispersion, characterized by Gd-rich regions and Gd-depleted zones. Comparative evaluation of Fig. 8b and c indicates that extending the homogenization time from 1 h to 80 h did not substantially enhance the uniformity of gadolinium distribution within the sintered pellets. This suggests that Gd_2O_3 agglomerates persist in the powder mixture despite prolonged low-energy mixing, leading to the observed EDS mapping patterns. Consequently, the morphology of the curves depicted in Fig. 7 remains unchanged, demonstrating the presence of the Kirkendall effect. The resultant sintered pellets exhibit reduced densities, attributed to the formation of stable pores at the sites of Gd_2O_3 agglomerates, which hinder densification during sintering. This observation is consistent with the findings reported by Durazzo et al. (2013), who identified that Gd_2O_3 agglomerates in UO_2-Gd_2O_3 fuel pellets lead to stable pore formation during sintering. These pores, originating from the Kirkendall effect due to differential diffusion rates between gadolinium and uranium, persist in the sintered structure, resulting in reduced pellet density.

Fig. 9 shows the effect of the energetic mixing time on the shrinkage curves (Fig. 9a) and rates (Fig. 9b) of samples S15, S30, and S60. Fig. 9a portrays an increase in shrinkage and a decrease in the inflection of the sintering curve with the increase in mixing time. Pellet S15 exhibited a typical shrinkage profile with the presence of agglomerates, as seen in Fig. 6a. The mixing time of 15 min in the HEM showed a comparable effect in the powder mixture to that in LEM (samples T1 and T80).

Extended homogenization durations during high-energy mixing (HEM) progressively enhanced the shrinkage behavior of UO_2–Gd_2O_3 fuel pellets. Notably, homogenization beyond 15 min altered the shrinkage rate profile, eliminating the previously observed two-stage shrinkage pattern associated with sintering blockage due to the Kirkendall effect. Fig. 9b illustrates that a dual-peak shrinkage rate occurred exclusively in the sample processed for 15 min. In contrast, samples mixed for 30 and 60 min exhibited a single, more pronounced shrinkage peak at lower temperatures, indicating improved densification. This behavior suggests that extended HEM effectively disrupts Gd_2O_3 agglomerates, enhancing powder homogeneity and mitigating the formation of stable pores that impede sintering.

Fig. 10 shows SEM images and EDS map of Gd of pure sintered UO_2 (Fig. 10a) and samples S15, S30, and S60 (Fig. 10b–c, and Fig. 10d, respectively). It is noted that the porosity of the sintered UO_2-Gd_2O_3 pellets decreased with increasing homogenization time. Fig. 10 also shows the chemical distribution of Gd in the sintered pellet. It is noticeable in the EDS maps that regions with many nearby pores are lighter in color, indicating the presence of Gd_2O_3 particles in the region. It can be observed that the longer the homogenization time the smaller the gadolinium concentration gradient, with darker regions (low in

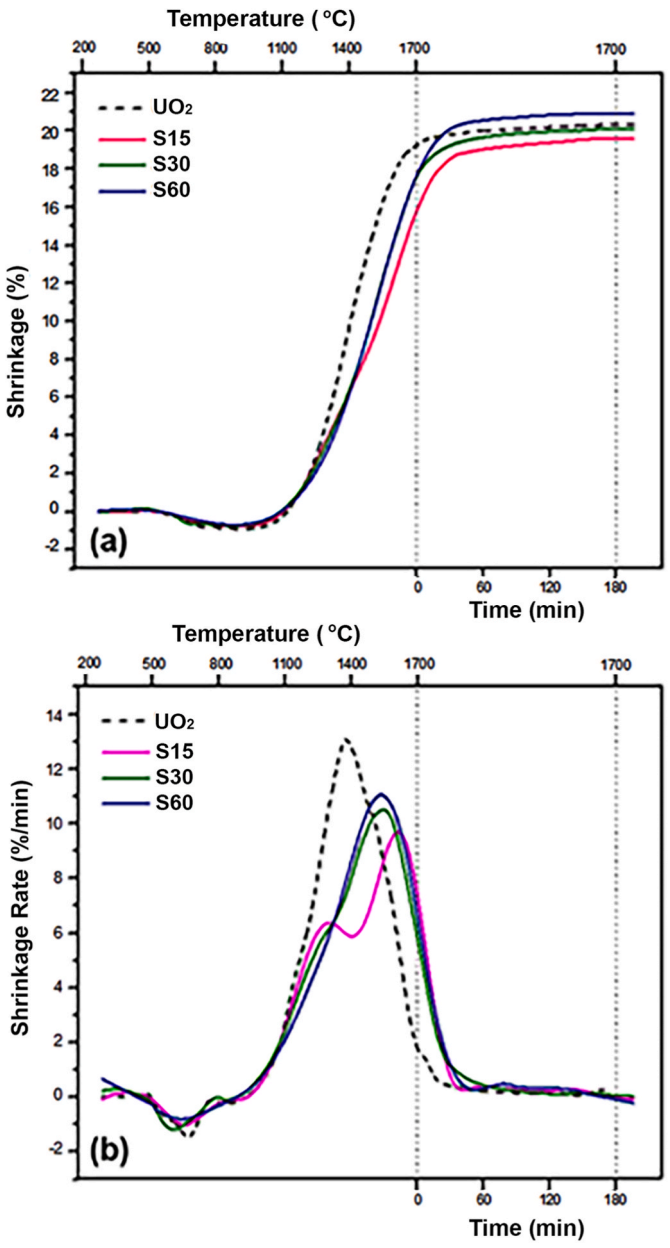

Fig. 9. Effect of adding 10 wt% Gd_2O_3 to the UO_2 pellet, with powders mixed in a HEM (Spex mixer) for 15, 30, and 60 min: (a) linear shrinkage, (b) shrinkage rate.

gadolinium) smaller in size and quantity, evidencing the improvement of the mixture's homogeneity.

Sintered densities are reported in Table 7. Dilatometry tests and density measurements show that the mixing time in the LEM did not influence the improvement of fuel pellet densification. With the use of a more vigorous homogenization procedure, the density after sintering increased significantly compared to the results obtained from pellets prepared by simple mechanical mixing in the LEM.

It is known that the presence of large Gd_2O_3 clusters increases the average pore sizes and decreases the sintered density (Durazzo et al., 2013; Balakrishna, 2016). Additional porosity is formed during solid solution formation, when the Kirkendall effect occurs. As Gd dissolves into the UO_2 matrix, a pore is formed at high temperatures, which cannot be closed. However, with the use of a more energetic mixing process, there is a reduction in the size of the Gd_2O_3 clusters, allowing for higher densities in sintered pellets. The specification for nuclear fuel stipulates a density above 93.5 %TD for commercial use (IAEA,1995). Therefore, the mixture made for 30 min in the HEM meets this specification.

The homogeneity of gadolinium (Gd) distribution within the UO_2 matrix is critical for ensuring a uniform neutronic response throughout the fuel pellet during irradiation. Due to the high thermal neutron absorption cross section of gadolinia, localized regions with elevated Gd concentrations experience a reduction in the neutron flux, thereby lowering the local fission rate and associated heat generation. As a result, such regions tend to exhibit reduced temperatures, potentially giving rise to internal thermal gradients in cases of non-uniform Gd distribution. A uniform dispersion of the neutron absorber not only contributes to a more consistent thermal profile throughout the pellet but also mitigates the formation of abnormally large pores during sintering.

4. Conclusion

The sintering behaviors of UO_2 and mixed UO_2 with 10 wt% Gd_2O_3 powders were investigated based on the energy and time of homogenization. From the results presented, the following aspects can be highlighted.

- The Kirkendall effect causes a decrease in pellet densification due additional porosity originated during solid solution formation. This effect is observed at 1200 °C, when the solid solution $(U,Gd)O_2$ starts to form.
- The efficiency of the mixture was analyzed by the shrinkage curves and rates in dilatometry as well as by EDS mapping of gadolinium. The formation of two peaks in the shrinkage rate curves in samples T1, T80 and S15 indicate the formation of Kirkendall pores during sintering. In heterogeneous mixtures, the EDS maps showed Gd-rich regions around the Kirkendall pores.
- Gadolinium acted as a densifying agent when its clusters are broken and distributed uniformly in the UO_2 powder during high-energy mixing.
- Dilatometric tests indicated that sintered UO_2-10 wt% Gd_2O_3 pellets mixed in LEM experienced a reduction in retraction due to the influence of the Kirkendall effect. It was evident that the mixing time did not have a substantial influence on the results.
- The HEM did not significantly alter the morphology of the UO_2 particles. With a mixing time greater than 30 min, it was possible to sinter UO_2-Gd_2O_3 pellets with a higher degree of homogeneity than the mixture in LEM, improving powder flowability and resulting in pellets with density within the specification range.
- The results demonstrate that increasing the mixing energy allow the UO_2 powder to maintain its flowability, compactability, and sinterability characteristics.

CRediT authorship contribution statement

Artur Cesar Freitas: Writing – original draft, Validation, Methodology, Investigation, Data curation, Conceptualization. **Diogo Ribeiro Costa:** Validation, Methodology, Formal analysis. **Ricardo Mendes Leal Neto:** Writing – review & editing, Validation, Methodology, Formal analysis, Conceptualization. **Elita Fontenele Urano de Carvalho:** Visualization, Validation, Investigation. **Michelangelo Durazzo:** Writing – review & editing, Validation, Supervision, Project administration, Conceptualization.

Data availability statement

The data that support the findings of this study are available from the corresponding author upon reasonable request.

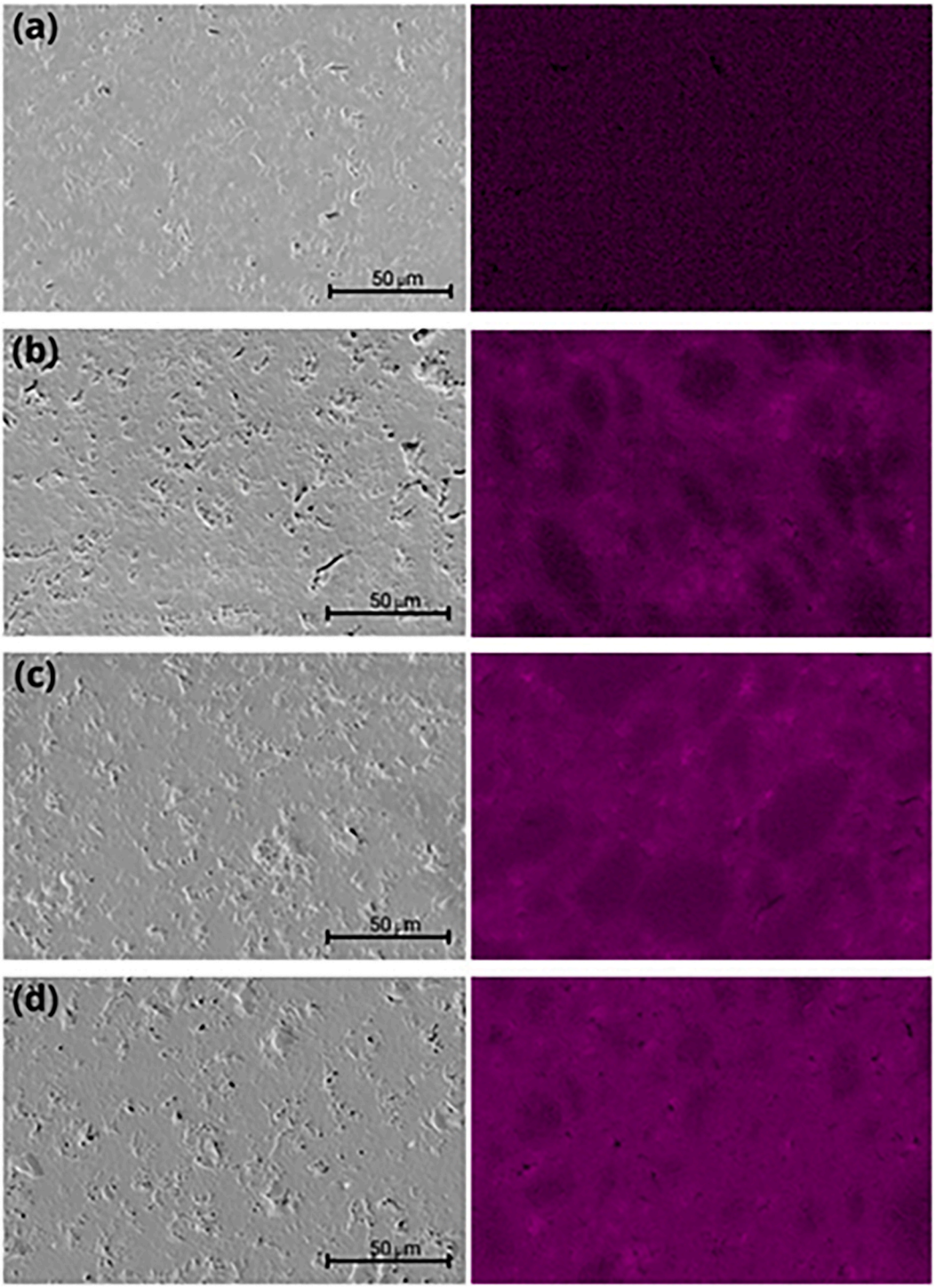

Fig. 10. SEM micrographs with secondary electron detector and EDS mapping of the UO_2 pellets (a), $(U,Gd)O_2$ – S15 (b), $(U,Gd)O_2$ – S30 (c), and $(U,Gd)O_2$ – S60 (d).

Table 7
Hydrostatic density of sintered pellets made with powders mixed in the LEM and HEM.

Pellet	sintered density (g/cm^3)	TD of the mixture (g/cm^3)	%TD
pure UO_2	10.36 ± 0.05	10.96	94.5 ± 0.4
T1	9.65 ± 0.02	10.62	90.8 ± 0.2
T80	9.66 ± 0.04	10.62	90.9 ± 0.4
S15	9.80 ± 0.05	10.62	92.2 ± 0.5
S30	10.12 ± 0.04	10.62	95.3 ± 0.3
S60	10.17 ± 0.04	10.62	95.8 ± 0.4

Declaration of competing interest

The authors declare that they have no known competing financial interests or personal relationships that could have appeared to influence the work reported in this paper.

Acknowledgements

The authors are grateful to CNPq (National Council for Scientific and Technological Development) for the research grant 309826/2021–7 provided for this work. The authors would also like to thank São Paulo

Research Foundation (FAPESP) for the research grant 2021/14331–5.

Data availability

Data will be made available on request.

References

American Society for Testing and Materials, 2021. ASTM International. Standard Specification for Sintered Gadolinium Oxide-Uranium Dioxide Pellets for Light Water Reactors - C922–21.

Assmann, H., Peehs, M., Roepenack, H., 1988. Survey of binary oxide fuel manufacturing and quality control. J. Nucl. Mater. 153, 115–126. https://doi.org/10.1016/0022-3115(88)90202-4.

Baena, A., Cardinaels, T., Govers, K., Pakarinen, J., Binnemans, K., Verwerft, M., 2015. Lattice contraction and lattice deformation of UO_2 and ThO_2 doped with Gd_2O_3. J. Nucl. Mater. 467, 135–143. https://doi.org/10.1016/j.jnucmat.2015.09.018.

Balakrishna, P., 2016. Fabrication of UO_2-Gd_2O_3 fuel pellets. J. Mater. Sci. Chem. Eng. 4 (2), 8–21. https://doi.org/10.4236/msce.2016.42002.

Beaunac, E., Leturia, M., Robisson, A.-C., Ablitzer, C., Saleh, K., 2022. Comparison of two powder conditioning methods to improve UO_2 powder flowability for press die filling. Powder Technol. 395, 1–13. https://doi.org/10.1016/j.powtec.2021.09.003.

Campolina, D., Faria, E.F., Santos, A.A.C., Vasconcelos, V., Franco, M.P.V., Dias, M.S., Mattos, J.R.L., 2018. Parametric study of enriched gadolinium in burnable neutron poison fuel rods for Angra-2. Ann. Nucl. Energy 118, 375–380. https://doi.org/10.1016/j.anucene.2018.04.025.

Cardinaels, T., Hertog, J., Vos, B., De Tollenaere, L., Delafoy, C., Verwerft, M., 2012. Dopant solubility and lattice contraction in gadolinia and gadolinia–chromia doped UO_2 fuels. J. Nucl. Mater. 424 (1–3), 289–300. https://doi.org/10.1016/j.jnucmat.2012.02.014.

Choi, C.S., Park, J.H., Kim, E.H., Shin, H.S., Chang, I.S., 1988. The influence of AUC powder characteristics on UO_2 pellets. J. Nucl. Mater. 153, 148–155. https://doi.org/10.1016/0022-3115(88)90206-1.

Coleman, S.C., Beeré, W.B., 1975. The sintering of open and closed porosity in UO_2. Philos. Mag. 31 (6), 1403–1413. https://doi.org/10.1080/00318087508228691.

Costa, D.R., Ezequiel, F.J., Gonzaga, R., Bernardelli, S.H., 2013. Individual influence of Al_2O_3 and Nb_2O_5 on grain growth of UO_2 sintered pellets manufactured at INB. In: International Nuclear Atlantic Conference. INAC, Recife, Brazil, 2013. (available at: http://www.iaea.org/inis/collection/NCLCollectionStore/_Public/45/087/45087491.pdf?r=1.

Costa, D.R., Freitas, A.C., 2017. Thermal stablitily test of UO_2-doped pellet manufactured at INB. In: International Nuclear Atlantic Conference - INAC. Belo Horizonte, Brazil, 2017. (available at: https://inis.iaea.org/collection/NCLCollectionStore/_Public/49/018/49018178.pdf.

Durazzo, M., Riella, H.G., 2001. Effect of mixed powder homogeneity on the UO_2-Gd_2O_3 nuclear fuel sintering behavior. Key Eng. Mater. 189–191, 60–66. https://dx.doi.org/10.4028/www.scientific.net/KEM.189-191.60.

Durazzo, M., Riella, H.G., 2009. Studies on the sintering behaviour of UO_2-Gd_2O_3 fuel pellets. In: IAEA-TECDOC-1654. Technical Committee Meeting on Advanced Fuel Pellet Materials and Fuel Rod Design for Water Cooled Reactors, Villigen, 23-26 Nov 2009, Switzerland. (available at: https://inis.iaea.org/records/n60xa-tc962.

Durazzo, M., Oliveira, F.B.V., Urano de Carvalho, E.F., Riella, H.G., 2010. Phase studies in the UO_2-Gd_2O_3 system. J. Nucl. Mater. 400, 183–188. https://doi.org/10.1016/j.jnucmat.2010.03.001.

Durazzo, M., Saliba-Silva, A.M., Urano de Carvalho, E.F., Riella, H.G., 2013. Sintering behavior of UO_2–Gd_2O_3 fuel: pore formation mechanism. J. Nucl. Mater. 433 (1–3), 334–340. https://doi.org/10.1016/j.jnucmat.2012.09.033.

Durazzo, M., Freitas, A.C., Sansone, A.E.S., Ferreira, N.A.M., Urano de Carvalho, E.F., Riella, H.G., Leal Neto, R.M., 2018. Sintering behavior of UO_2-Er_2O_3 mixed fuel. J. Nucl. Mater. 510, 603–612. https://doi.org/10.1016/j.jnucmat.2018.08.051.

Fedotov, A.V., Mikheev, E.N., Lysikov, A.V., Novikov, V.V., 2013. Theoretical and experimental density of (U,Gd)O_2 and (U,Er)O_2. Atom. Energy 113 (6), 429–434. https://doi.org/10.1007/s10512-013-9657-3.

Fruhstorfer, J., Aneziris, C.G., 2017. Influence of particle size distributions on the density and density gradients in uniaxial compacts. Ceram. Int. 43 (16), 13175–13184. https://doi.org/10.1016/j.ceramint.2017.07.011.

Fukushima, S., Ohmichi, T., Maeda, A., Watanabe, H., 1982. The effect of gadolinium content on the thermal conductivity of near-stoichiometric (U,Gd)O_2 solid solutions. J. Nucl. Mater. 105 (2–3), 201–210. https://doi.org/10.1016/0022-3115(82)90375-0.

Glodeanu, F., Spinzi, M., Bălan, V., 1988. Correlation between UO_2 powder and pellet quality in PHWR fuel manufacturing. J. Nucl. Mater. 153, 156–159. https://doi.org/10.1016/0022-3115(88)90207-3.

Hirai, M., Ishimoto, S., 1991. Thermal diffusivities and thermal conductivities of UO_2-Gd_2O_3. J. Nucl. Sci. Technol. 28 (11), 995–1000. https://doi.org/10.1080/18811248.1991.9731462.

Ho, S.M., Radford, K.C., 1985. Structural chemistry of solid solutions in the UO_2-Gd_2O_3 system. Nucl. Technol. 73 (3), 350–360. https://doi.org/10.13182/NT86-A16077.

Hume-Rothery, W., 1966. Atomic diameters, atomic volumes and solid solubility relations in alloys. Acta Metall. 14 (1), 17–20. https://doi.org/10.1016/0001-6160(66)90267-7.

International Atomic Energy Agency IAEA, 1995. Characteristics and use of urania-gadolinia fuels, 1995 International Atomic Energy Agency. IAEA-TECDOC-844., Vienna. available at: https://inis.iaea.org/records/43bpj-qdb30.

Jentzen, W.R., Didway, J.A., 1990. Method of making a UO_2 fuel pellet. European Patent Application EP 0395979A1 (available at: https://patents.google.com/patent/EP0395979A1/en.

Kim, J.H., Song, K.W., Kang, K.W., Yang, J.H., Kim, J.H., 2001. Sintering of a mixture of UO_2 and Gd_2O_3 powders doped with Cr_2O_3-S_iO_2. J. Korean Nucl. Soc. 33 (4), 386–396 (available at: https://www.kns.org/files/jour/v33/A04803285910.pdf.

Leyva, A.G., Vega, D., Trimarco, V., Marchi, D., 2002. Homogeneity characterization of sintered (U,Gd)O_2 pellets by X-ray diffraction. J. Nucl. Mater. 303, 29–33. https://doi.org/10.1016/S0022-3115(02)00819-X.

Madian, A., Leturia, M., Ablitzer, C., Matheron, P., Bernard-Granger, G., Saleh, K., 2020. Impact of fine particles on the rheological properties of uranium dioxide powders. Nucl. Eng. Technol. 52 (8), 1714–1723. https://doi.org/10.1016/j.net.2020.01.012.

Manzel, R., Dörr, W.O., 1980. Manufacturing and irradiation experience with UO_2/Gd_2O_3 fuel. Am. Ceram. Soc. Bull. 59 (6), 601–603 (abstract available at: https://www.osrrti.gov/biblio/5280816.

Mills, K.C., Ponsford, F.H., Richardson, M.J., Zaghini, N., Fassina, P., 1989. Heat capacity and enthalpy of UO_2 and gadolinia-doped UO_2. Thermochim. Acta 139, 107–120. https://doi.org/10.1016/0040-6031(89)87014-5.

Pagano, L., Valença, G.P., Silva, S.L., Claudio, A.E.L., Ivashita, F.F., Barco, R., Medeiros, S.N., Paesano, Jr. A., 2008. Mössbauer study and structural characterization of UO_2–Gd_2O_3 sintered compounds. J. Nucl. Mater. 378 (1), 25–29. https://doi.org/10.1016/j.jnucmat.2008.03.024.

Radford, K.C., Pope, J.M., 1983. UO_2 fuel pellet microstructure modification through impurity additions. J. Nucl. Mater. 116 (2–3), 305–313. https://doi.org/10.1016/0022-3115(83)90116-2.

Restivo, T.A.G., Claudio, A.E.L., Silva, E.D., Pagano, Jr. L., 2004. Effect of additives on the sintering kinectics of the UO_2-Gd_2O_3 system. In: IAEA-TECDOC-1416, Advanced Fuel Pellet Materials and Designs for Water Cooled Reactors. IAEA, Vienna, 2004. (available at: https://www-pub.iaea.org/MTCD/publications/PDF/TE_1416_web.pdf.

Riella, H.G., Durazzo, M., Hirata, M., Nogueira, R.A., 1991. UO_2-Gd_2O_3 solid solution formation from wet and dry processes. J. Nucl. Mater. 178 (2–3), 204–211. https://doi.org/10.1016/0022-3115(91)90387-M.

Santos, L.R., Durazzo, M., Urano de Carvalho, E.F., Riella, H.G., 2017. Effect of $Al(OH)_3$ on the sintering of UO_2–Gd_2O_3 fuel pellets with addition of U_3O_8 from recycle. J. Nucl. Mater. 493, 30–39. https://doi.org/10.1016/j.jnucmat.2017.05.050.

Shannon, R.D., 1976. Revised effective ionic radii and systematic studies of interatomic distances in halides and chalcogenides. Acta Crystallogr. A32, 751–767. https://doi.org/10.1107/S0567739476001551.

Song, K.W., Kim, K.S., Yang, J.H., Kang, K.W., Jung, Y.H., 2001. A mechanism for the sintered density decrease of UO_2–Gd_2O_3 pellets under an oxidizing atmosphere. J. Nucl. Mater. 288 (2–3), 92–99. https://doi.org/10.1016/S0022-3115(00)00721-2.

Yaws, C.L., 2015. Yaws Handbook of Physical Properties for Hydrocarbons and Chemicals, 2015. Gulf Professional Publishing, Houston, Texas, p. 687 (available at: https://www.sciencedirect.com/book/9780128008348/the-yaws-handbook-of-physical-properties-for-hydrocarbons-and-chemicals#book-description.

Yuda, R., Une, K., 1991. Effect of sintering atmosphere on the densification of UO_2-Gd_2O_3 compacts. J. Nucl. Mater. 178 (2–3), 195–203. https://doi.org/10.1016/0022-3115(91)90386-L.